Characterisation of ultrasonic structural noise in multiple scattering media using phased arrays

Thomas Bedetti, Vincent Dorval, Frédéric Jenson, Arnaud Derode

Journal of Physics: Conference Series **457** (2013) 012003 doi:10.1088/1742-6596/457/1/012003

Characterisation of ultrasonic structural noise in multiple scattering media using phased arrays

T Bedetti[1], V Dorval[1], F Jenson[1] and A Derode[2]

[1] CEA, LIST, F-91191, Gif-sur-Yvette cedex, France
[2] Institut Langevin, Université Paris Diderot – Paris 7, ESPCI ParisTech, CNRS UMR 7587, 10 rue Vauquelin, 75005 Paris, France

E-mail: thomas.bedetti@cea.fr, vincent.dorval@cea.fr

Abstract. The ultrasonic inspection of multiple scattering media gives rise to structural noise which makes it difficult to detect potential damage or crack inside the component. In order to predict the performances of ultrasonic inspection over such complex media, scattering models can be used. Such models rely on specific key parameters describing the multiple scattering process, which can be determined by specific measurements and post-processing techniques. Such experiments were carried out on stainless steel plates using linear phased-arrays. They consist in recording the response matrix constituted by impulse responses between all the elements of the array. By conducting post-processing on this matrix, we measure the elastic mean free path l_e and the correlation distance d_c of the recorded noise. Additionally, the dynamic behaviour of the coherent backscattering effect was studied in order to measure the diffusion constant D. Plane-wave beamforming has been applied to the response matrix to improve the angular resolution and the signal-to-noise ratio of the backscattered intensity. Details of post-processing techniques will be shown.

1. Introduction

In the context of Non Destructive Testing (NDT), the acoustical inspection of scattering media represents a scientific challenge. Such materials are widely used in the industry, from stainless steel pipes used in nuclear power plants to concretes and composite materials used respectively in construction and aeronautical industries. Due to their complex microstructure, they are difficult to inspect. Indeed, the interaction of an ultrasonic wave with the microstructure leads to the deformation of the incident beam by scattering. In the case of stainless steels, the grain boundaries act as an impedance contrast. When the wavelength is of the same order of magnitude as the size of these grains, the wave is scattered and its energy is spread over the medium, attenuating the incident beam and making a "structural noise" appear. The amplitude of this noise can even become higher than echoes corresponding to the presence of defects in the structure. In this case, the quality of the inspection is compromised. Two main phenomena contribute to the noise: single scattering, when only one scatterer has been involved before the recording of the wave, and multiple scattering, when the wave is scattered several times along its path. There is no clear limit between these two regimes but it is sometimes possible to neglect one of the contributions in comparison to the other.

Simulations are often used to evaluate the detection capabilities of inspection methods. For this purpose, CIVA, the NDT simulation software developed at the CEA, includes different models that simulate the propagation of ultrasonic waves in various media. In the case of polycrystalline structure,

a noise generator based on the single scattering hypothesis has been developed [1]. Nevertheless, when multiple scattering effects cannot be neglected, the noise level is underestimated. A new noise simulation method is currently developed to take these effects into account. Contrary to numerical approaches such as finite element methods [2], it uses a semi analytical approach to model multiple scattering. It requires parameters that characterize the scattering as input.

The propagation of ultrasonic waves in the multiple scattering regime has been widely studied. Turner and Weaver proposed a study of the incoherent intensity propagation in polycrystalline materials based on the Radiative Transfer Equation [3]. Also, Page tested the diffusion approximation to describe the propagation trough a random medium [4]. In these models, it is common to characterise the transport properties in a disordered medium in terms of the elastic mean free path l_e, the transport mean free path l^* and the diffusion constant D. In addition, Derode studied the statistics of speckle patterns obtained by recording structural noise [5]. Though this study was limited to single scattering in anisotropic composites, Derode showed that the correlation distance of the noise d_c was influenced by the microstructure. The new simulation method takes these three parameters as entry values.

However, the experimental determination of l_e , D and d_c classically needs different setups. In this paper, we show that it is possible to estimate the three parameters via one single recording. In NDT, N-element phased arrays are more and more used to inspect structures. A widely used process is to perform the so-called Full Matrix Capture (FMC) to record the response matrix K of the array, which contains all the impulse responses between every element of the array. By applying post-processing techniques to K, it is possible to extract various data. The study of the coherent field can lead to l_e, of the incoherent field to d_c, and of the intensity to D by highlighting the coherent backscattering effect.

2. Experimental setup and post-processing techniques

In the experiment, the transducer and the sample are placed in a water tank. We used two N-element ultrasonic arrays whose characteristics are described in table 1. The sampling frequency is 40MHz.

The experiment consists in measuring the response matrix K, i.e. the interelement matrix of the array (see figure 1). A 2-period-long sine is emitted from transducer e into the scattering sample. The backscattered wave is recorded with the N transducers of the same array. The operation is repeated for the N emitting transducers. The NxN array response matrix $K(t)$ whose elements are the N^2 impulse responses $k_{er}(t)$ is finally obtained. The entire measure is then repeated for P positions of the array, in order to perform averaging over the distribution of the scatterers into the medium.

The recording of K is done in two forged stainless steel plates. These plates have the same thickness d = 24mm and differ in the size of their grains γ, 130µm and 500µm. From here on, they will be called, respectively, SG (Small Grains) and CG (Coarse Grains) samples. The elastic properties of the plates can be found in table 2. The distance between the sample and the array is h = 100mm. The number of positions of the array differs according to the sizes of the sample. 55 matrices are recorded in the CG sample and 90 in the SG sample.

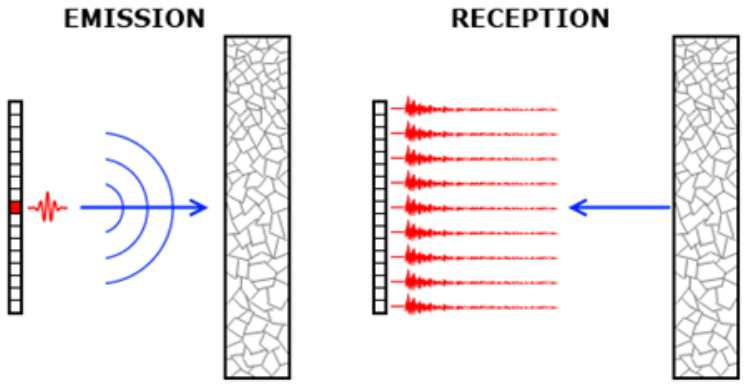

Figure 1. Experimental setup.

Table 1. Characteristics of the linear phased arrays.

Reference	Central frequency	-6dB Bandwidth	*N*	Element size	Pitch	Array size
SONO12	1.5 MHz	1.2 – 1.9 MHz	64	0.5 x 12 mm	0.55 mm	35.15 mm
SONO65	3 MHz	2 – 3.8 MHz	64	0.389 x 12 mm	0.417 mm	26.66 mm

Table 2. Elastic properties of the forged stainless steel plates.

v_L	v_T	ρ	C_{11}	C_{12}	C_{44}
5650 m.s^{-1}	3100 m.s^{-1}	8.12 g.cm^{-3}	169 GPa	145 GPa	123 GPa

In order to obtain the searched parameters, we chose to perform beamforming to the response matrix, as is usually done with ultrasonic arrays for instance in medical imaging [6]. By applying delay laws along the dimensions of *K*, it is possible to simulate various experimental setups:

- Far field conditions using plane waves.
- Near field conditions using virtual point source.
- Focused transducers using cylindrical delay laws.

In this paper, we will use plane wave beamforming. First, we introduce a linear delay between impulse responses $k_{er}(t)$ so that signals from the required directions are brought into phase. Second, the time-shifted signals are added. At the cost of longer computation times than direct measurements, the signal to noise ratio is higher due to the fact that every impulse response contributes to the final signal $s_{\alpha\beta}(t)$, with α and β the angles of interest respectively in emission and reception.

Without additional correction, and due to the finite size of the array, edge effects can disturb the precision of the beamforming. To correct it, apodisation is performed with the help of a Hann window to assure the planarity of the emitted wave.

3. Determination of the parameters

3.1. Coherent field and elastic mean free path

During the propagation of an ultrasonic wave in a polycrystalline medium, each scattering that occurs leads to the spreading of a part of the energy over the sample. In consequence, the intensity of the coherent wave that resists to averaging is progressively attenuated. The characteristic distance of this attenuation is called the elastic mean free path, l_e. It is assumed that attenuation by intrinsic absorption is negligible compared to attenuation by scattering.

Knowing the value of l_e and the thickness d of the plate, the ratio l_e/d is a useful information about the scattering regime inside the medium [7]. If it is above one, the coherent wave is still dominant and multiple scattering can be neglected. On the contrary, if it is less than one, the coherent wave lost the majority of its energy by the time it reaches the back-surface of the plate. In that case, single scattering becomes negligible and multiple scattering dominates. This regime is often called the "diffusion regime" due to the way the acoustic energy is propagating into the medium. More information will be found in paragraph 3.3.

Classically, the measure of l_e is done using a transmission setup, working on samples of different thicknesses. Here, as we impose the use of the response matrix obtained in reflection, the calculation method is based on the study of the two first back-wall echoes spectra [8]. Taking into account absorption, attenuation, and the interface between the couplant and the medium, we can write the amplitude of the two echoes spectra of a plane wave emitted at zero incidence as a function of the incident wave $|A_0(\omega)|$.

$$|A_{echo\,1}(\omega)| = |A_0(\omega)|\, e^{-2\alpha_1(\omega)h}\, e^{-2\alpha_2(\omega)d}\, T_{12}R_{22}T_{21} \quad (1)$$

$$|A_{echo\,2}(\omega)| = |A_0(\omega)|\, e^{-2\alpha_1(\omega)h}\, e^{-4\alpha_2(\omega)d}\, T_{12}R_{22}^3T_{21} \quad (2)$$

where α is the attenuation coefficients, T and R are the transmission and reflection coefficients, and the subscripts 1 and 2 correspond respectively to the coupling medium and the sample, as the back-wall medium is the same as the couplant. Dividing one expression by the other, we obtain a realisation of the attenuation function of the coherent field, $\alpha_2(\omega)$. As the elastic mean free path is the characteristic distance of attenuation of the intensity, it is proportional to the inverse of the attenuation function:

$$l_e(\omega) = \frac{1}{2\alpha_2(\omega)} = d\left[\ln(R_{22}^2) + \ln\left(\frac{|A_{echo\,1}(\omega)|}{|A_{echo\,2}(\omega)|}\right)\right]^{-1} \tag{3}$$

In order to measure this value from the response matrix, the following process is followed. The first step is to perform a plane wave beamforming at zero incidence, meaning that the matrix K is summed along the emitters and the receivers without applying any delay law. The second step, leading to the determination of the coherent signal $A_{coh}(t)$, is to average over disorder, represented by the P positions of the array.

$$A_{coh}(t) = \langle \sum_{e,r} k_{er}(t) \rangle_P \tag{4}$$

Coherent waves calculated for both plates and both transducers are shown on Figure 2. It shows that according to grain size and frequency, the numbers of echoes that we are able to observe may vary. In the case of the SG sample, more than two echoes are detected whatever the frequency. On the contrary in the CG sample, the first two echoes are visible using the SONO12 array (c), but with the SONO65, the second one do not comes out of the noise (d). That means that in this plate, multiple scattering dominates very quickly at 3MHz.

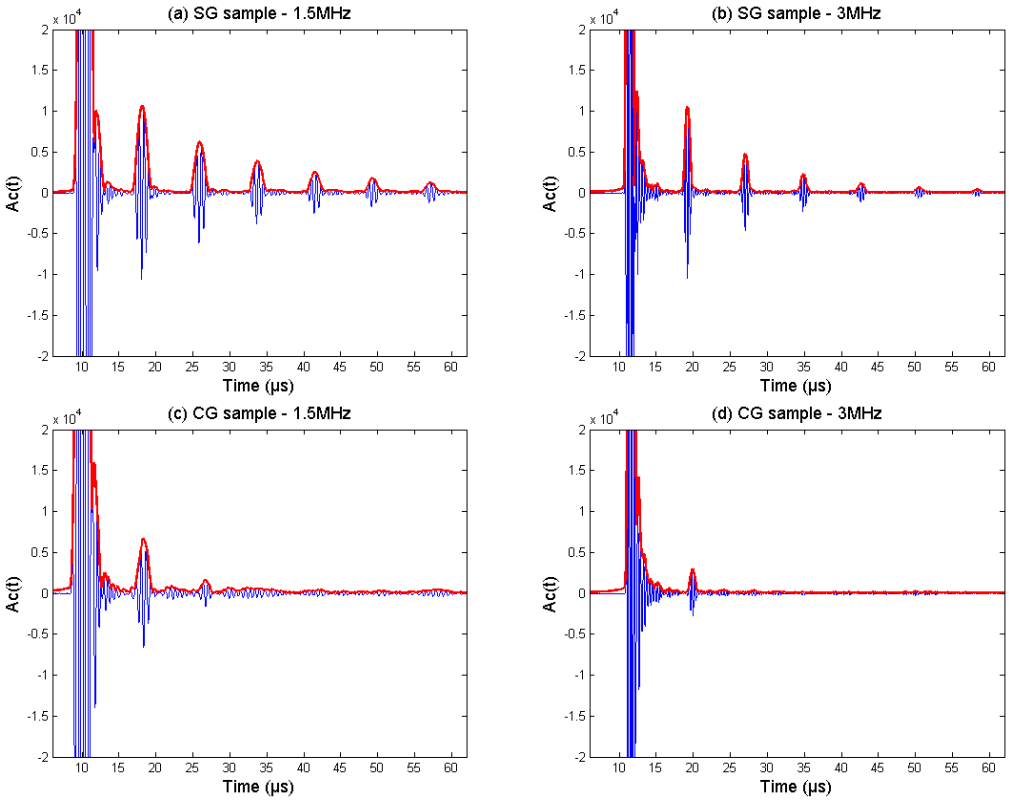

Figure 2. Coherent waves obtained for each couple sample-array: SG plate with SONO12 (a) and SONO65 (b); CG plate with SONO12 (c) and SONO65 (d).

The third step is to take the Fourier transform of the echoes. At last, using equation (3), we can calculate l_e, whose behaviour with frequency is shown on figure 3. For the SG plate, we observe the decrease of l_e with frequency. This is consistent with the fact that at lower λ/γ ratio, scattering effects are more important. For the CG plate, the same decrease is observed with the SONO12 array. Unfortunately, the thickness of the sample prevented the detection of the second back-surface echo, making it impossible to calculate l_e. This problem could be solved by testing samples with a lower thickness. Doing so will increase the ratio l_e/d and extend the numbers of visible echoes. However, this is not the best solution in the idea of a unique experimental setup as we will see in the following paragraphs how the back-surface echoes can limit the measure of the other parameters.

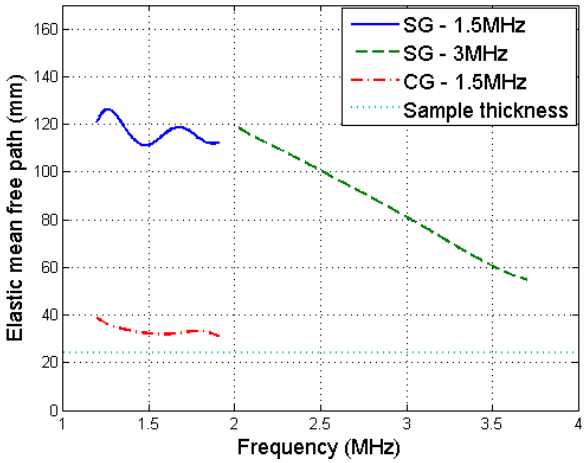

Figure 3. Elastic mean free path as a function of frequency in the steel samples.

3.2. Incoherent field and noise correlation distance

The recorded noise appears as a speckle pattern. By studying its spatial variations, it is possible to extract a characteristic size of its spots. We call this size the correlation distance d_c. It represents the fact that even if the noise appears to be random, two signals close to each other will show similarities. For simulation purpose, knowing its value will give information about the spatial behaviour of the phase term of the backscattered field.

During the study of the elastic mean free path, the calculation was made on the coherent wave. Here, we will be processing the incoherent wave. The aim is to get rid of the back-surface echoes, because their presence could compromise the calculation by introducing correlations at long distance that are not relevant in the speckle statistics. However, back-wall echoes are not the only contributions that are subtracted from the signals as it is known that the ballistic wave, which seems to propagate as if it was in a homogeneous medium, is only a part of the coherent wave [9].

The first step of the post-process is the same as for the mean free path, i.e. zero incidence beamforming is performed. But this time the sum is only made on emission, to obtain a B-scan where each signal is the sum of the coherent and the incoherent waves. To isolate the incoherent part $A_{inc}(t,r)$, the average of the B-scans over the positions of the array is subtracted:

$$A_{inc}(t,r) = \sum_e k_{er}(t) - \langle \sum_e k_{er}(t) \rangle_P \tag{5}$$

For every couple of elements r_i and r_j distant of δ from each other, we then calculate the cross-correlation at zero lag:

$$\varepsilon(\delta) = R_{x_i x_j}(0) = \int x_i^*(\tau) x_j(\tau)\, d\tau \tag{6}$$

where x_i and x_j are respectively the signals recorded by r_i and r_j. Finally, for each value of δ, ε is normalised by the number of occurrences of the inter-element distance. The resulting function is plotted on figure 4, for the CG plate and the SONO65 array (3MHz). It shows that the correlation of the signals along the length is well described by an exponential decay. By fitting the resulting curve with an exponential test function f, it is possible to deduce the value of d_c:

$$f(\delta) = a\, e^{-b.\delta} \quad , \quad (a,b) > 0 \quad \rightarrow \quad d_c = \frac{1}{b} \tag{7}$$

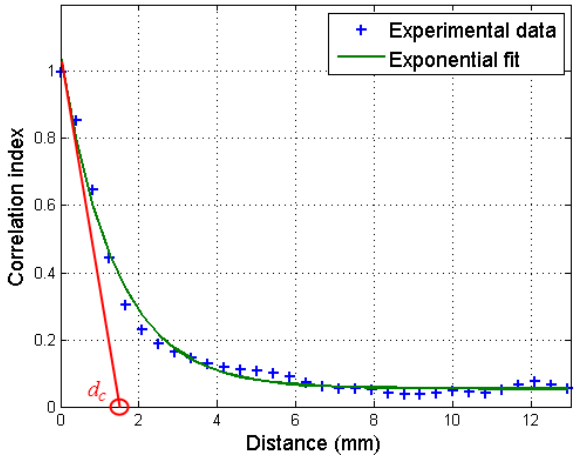

Figure 4. Normalised cross-correlation at zero lag as a function of inter-element distance for the CG sample at 3MHz.

The value of the correlation distance obtained by this method corresponds to the whole signal recorded by the array. However, its behavior with time is not determined that way. To access this information, the same calculation is done on 5-µs-long overlapping time windows δt:

$$\varepsilon(\delta, T) = \int_{T}^{T+\delta t} x_i^*(\hat{\tau}) x_j(\hat{\tau})\, d\hat{\tau} \tag{8}$$

The dependence of the correlation distance with time is calculated by applying the exponential fit at each step T of time. The result is shown on figure 5. In the CG sample (figure 5(a) and 5(b)) the spatial correlation of the structural noise is decreasing over time. However, it is not possible to ensure that it tends to zero, as the spatial resolution is limited by the pitch of the array. The local maxima that appear around 18µs and 25µs denote the persistence of the back-surface echoes even after the subtraction of the mean of the field. This is due to the deformation of the wavefront during the propagation in the scattering medium. The back-surface echo lost a part of its coherence and cannot be entirely eliminated. More averaging, or a more appropriate time-gating, would be required to gain a better correction.

In the SG sample (figure 5(c) and 5(d)) the same general behavior is obtained, but the prominence of the back-wall echoes over the incoherent wave is greater than in the CG samples. The long-distance correlations induced this way make the evolution of d_c poorly visible in these samples, and at these frequencies.

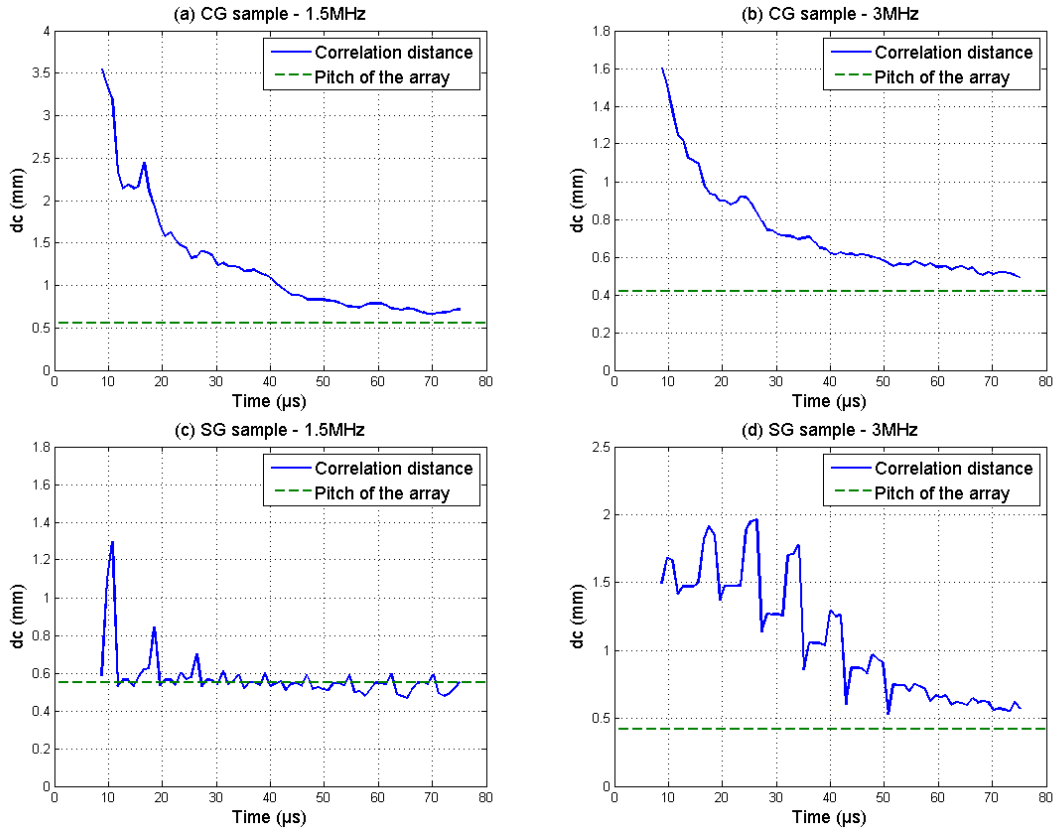

Figure 5. Correlation distance of the noise as a function of time. CG plate with SONO12 (a) and SONO65 (b); SG plate with SONO12 (c) and SONO65 (d).

3.3. Incoherent intensity and diffusion constant

As we saw in the first paragraph, after several mean free paths, the multiple scattering regime become dominant and the coherent wave is greatly attenuated. Indeed, the ultrasonic energy has been transferred to the incoherent wave, creating a halo spreading into the medium. The propagation of this halo can be treated as a random walk [4]. Under this approximation, called the diffusion approximation, the energy density over disorder obeys to the diffusion equation:

$$D\,\Delta\langle I(r,r',t,t')\rangle - \frac{\partial\langle I(r,r',t,t')\rangle}{\partial t} = \delta(r-r')\delta(t-t') \tag{9}$$

where I is the energy density of the wave, D is the diffusion constant and (r',t') is the position of the diffuse source in space and time. The diffusion constant is a dynamic parameter related to the growth speed of the diffusive halo. To infer the value of D from the response matrix, we will study the coherent backscattering effect. It highlights the long-time persistence of coherent interferences even in a disordered media. This effect corresponds to an enhancement in the intensity of waves that are backscattered along the incidence direction. Considering two scattering paths p and q into the medium (see figure 6(a)), the calculation of the average backscattered intensity leads to:

$$\langle I\rangle = \sum_p \langle |A_p|^2\rangle + \sum_p \sum_{q\neq p} \langle A_p^* A_q\rangle = I_{inc} + I_{coh} \tag{10}$$

where A is the amplitude of the considered path. The first term corresponds to the sum of individual intensities of each path. The contribution of this term to the total intensity will not present angular

variations, at least in the far field and at small angles. The second term originates from the interference between different scattering paths. As an average over disorder is performed, the mean value of I_{coh} is zero in the general case because each path is uncorrelated with every other one. However, when source and receiver coincide, each multiple scattering path has a twin brother (its reciprocal counterpart, meaning that the same scatterers come into play but in the opposite order) and both path are necessarily in phase (figure 6(b)). Therefore at exact backscattering (i.e. θ = 0, source = receiver) happens a coherent interference. Thus, $I_{coh} \approx I_{inc}$ and the mean intensity is higher by a factor 2. The angular width $\Delta\theta$ of the peak essentially depends on the conditions (far- or near-field), the wavelength and the transport parameters (D, l_e, l^*) of the multiple scattering medium.

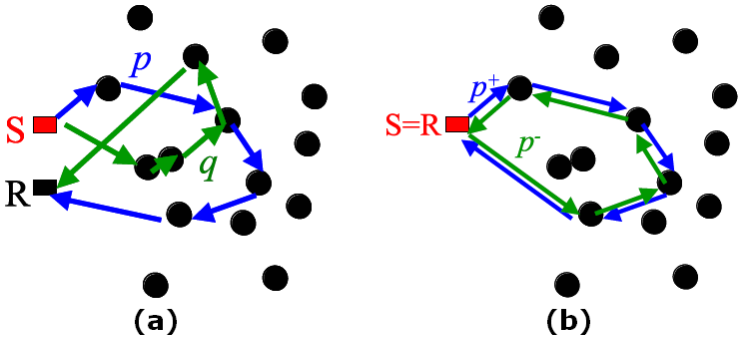

Figure 6. (courtesy of A. Aubry) Interferences (a) between uncorrelated scattering paths and (b) between reciprocal paths.

It has been shown [10] that under the far-field condition and in diffusive regime, the coherent backscattering spot width narrows with time:

$$\Delta\theta(t) \propto \frac{h}{k\sqrt{Dt}} \quad \text{with} \quad h \gg \sqrt{Dt} \tag{11}$$

where $\Delta\theta$ is the half-width at half-maximum of the coherent peak, h is the distance between the array and the sample, and k is the wavenumber in water. The recording of the backscattering peak and the study of its angular evolution with time will then give us access to D performing a linear fit of the inverse square of the half-width at half-maximum with respect to time:

$$\Delta\theta^{-2} = \frac{k^2 D}{\Gamma} t \tag{12}$$

where Γ is a factor which depends on the distance h and on the directivity of the transducers.

In this paragraph, we will compare two ways of computing the average backscattered intensity from the response matrix $K(t)$. These post-processing techniques are adapted from the work of A. Aubry on randomly located steel rods immersed in water [11]. The linear fit will be performed on both coherent backscattering peaks to compare the two methods.

The first and usual way to obtain the coherent peak is to work directly on the recorded signals $k_{er}(t)$. First, the signals are time shifted in reception to compensate for the different arrival times between the elements of the array. The intensity is then calculated by integrating the square of the signals on overlapping time windows. An average is then performed over all element couples in emission/reception that correspond to the same backscattering angle. Then another averaging is performed over the P positions of the array:

$$I_1(\theta, T) = \langle |k_{er}(t - \Delta t_{er})|^2_{t-\Delta t_{er}\, \epsilon\, [T;T+\delta t]} \rangle_P \tag{13}$$

where Δt_{er} is the arrival time correction between the two signals, δt is the length of the time window, and θ = Arctan[(*e*-*r*).*p*/*h*] with *p* the pitch of the array. Figure 7(a) shows a result for the averaged backscattered intensity from the CG sample at 3MHz.

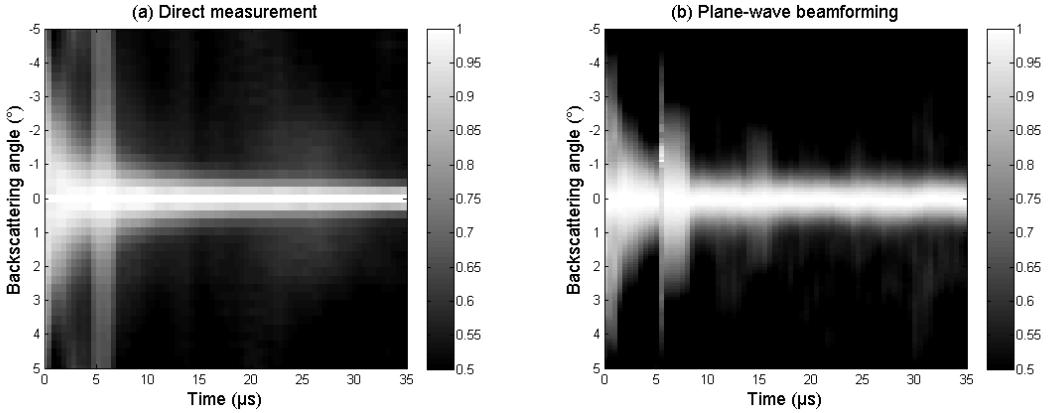

Figure 7. Dynamic backscattered intensity obtained from direct measurement (a) and from plane-wave beamforming technique (b) in the CG sample at 3MHz. At each time step, the intensity is normalised by its maximum along the backscattering angle.

In this figure, the intensity is normalized at each time step by its maximum for this time. This maximum always occurs around the 0° backscattering angle because this is where the coherent backscattering effect is most significant. The measurement is affected by a presence of a backwall echo around 6µs. For the rest of the time interval the width of the peak decreases regularly, as expected.

The other way to compute the coherent backscattering peak is to use plane-wave beamforming. As explained in section 2, the principle is to apply delay laws to the signals to simulate the emission and reception along different angles. Additionally, the use of plane-waves is a way to ensure that the far-field condition, required to observe the decrease of the peak's width, is fulfilled. It is possible to work in the time domain or in the Fourier space. In the time domain, a small variation of angle implies the application of a delay that can be lower than the sampling time. On the contrary, applying delay laws in the frequency domain reduces the operation to a simple matrix multiplication. For this reason, we chose to work in Fourier space. First, a fast Fourier transform gives the response matrix $K(f)$ in the frequency domain. Then, considering the emission along the angle α and the reception along the angle β, the delay laws are calculated for each element of the array with the first transducer taken as reference:

$$\begin{cases} \tau_\alpha(e) = \dfrac{(e-1)p\sin\alpha}{c} \\ \tau_\beta(r) = \dfrac{(r-1)p\sin\beta}{c} \end{cases} \tag{14}$$

where *c* is the velocity of the wave in the coupling medium. Next, we take the Fourier transform of these laws:

$$\begin{cases} \tilde{\tau}_\alpha(f,e) = e^{-2i\pi f\tau_\alpha(e)} \\ \tilde{\tau}_\beta(f,r) = e^{-2i\pi f\tau_\beta(r)} \end{cases} \tag{15}$$

After that, we calculate the matrix multiplication for each frequency to obtain the signal integrated by the array after the emission along α and the reception along β.

$$s_{\alpha,\beta}(t) = TF^{-1}\left[\tilde{\tau}_\alpha(f,e) * \tilde{k}_{er}(f) * {}^t\tilde{\tau}_\beta(f,r)\right] \tag{16}$$

The dynamic intensity $I_2(\theta,T)$ is finally obtained by integrating the square norm of $s_{\alpha,\alpha+\theta}(t)$ over overlapping time windows and by averaging over the emission angle α and the P positions of the array. The result calculated in the CG sample at 3MHz is shown on figure 7(b).

$$I_2(\theta,T) = \langle \left| s_{\alpha,\alpha+\theta}(t) \right|^2_{t\,\epsilon\,[T;T+\delta t]} \rangle_{\alpha,P} \tag{17}$$

The study of the direct measurement peak (figure 7(a)) shows the enhancement by a factor 2 of the backscattered intensity. Moreover, with this method, the angular resolution is limited by the pitch of the array. Indeed, it is impossible to get information below the angle p/h, limiting the range of calculation of D.

Using plane-wave beamforming, we see that there is less energy along the higher backscattering angles, meaning that the signal-to-noise ratio has been increased. It is the consequence of the use of every impulse responses contained in the response matrix to determine a single signal. Additionally, it is theoretically possible to improve the angular resolution and to access long time information about the angular variation of the backscattering peak. However, a saturation phenomenon is quickly observed. Indeed, in the far field setup, the angular resolution is dependant of the aperture of the array and the saturation occurs when the width of the peak reach λ/Np. In our experimental setup, the size of the available array (≈27mm), associated with a 3MHz pulse, leads to a limit of 1°. This value is consistent with the experimental result presented on figure 7(b) as we see that the total width at half-maximum (i.e. for an amplitude of 0.75) is 1°. Increasing the size of the array should improve the angular resolution.

Finally, we see that with both techniques the presence of the first back-surface echo is a limiting factor. On the one hand, its presence prevents the visualisation of the peak evolution. On the other hand, the behaviour of noise could be modified due to the backwall reflection that will bring more energy to the diffuse field as it propagates again through the medium. Thus, the determination of D will be done in the time interval before the apparition of the back-surface echo.

Before extracting the value of D from the coherent backscattering peak, we have to verify the applicability of equation (11). Indeed, this equation is only valid in the diffusion approximation. To that aim, we verify the time dependence of the peak's width decrease. If the diffusion approximation is valid, the slope of the linear fit of $\log(\Delta\theta)$ with respect to $\log(t)$ must be equal to -0.5. The result of the calculation is plotted on figure 8.

For direct measurement, the slope is inferior to the expected value, but with beamforming, we obtain a good agreement with the theory. That means that the determination of the diffusion constant is more likely to be precise with the beamforming treatment. It also indicates that though there is undoubtedly multiple scattering, the truly diffuse regime is probably not attained. In that case the energy spreads from the source in a manner not as simple as $\sqrt{Dt}$ and is more accurately described by the radiative transfer equation [3].

Finally, D is obtained by the linear regression of the inverse square of the half-width at half-maximum with respect to time (equation (12)). The slope of this regression leads to the diffusion constant as:

$$D = \frac{ah^2\Gamma^2}{k^2} \tag{18}$$

The results of the two regressions are plotted on figure 8. The values obtained are:

$$\begin{cases} D_1 = 7.5\, mm^2/\mu s \\ D_2 = 6.3\, mm^2/\mu s \end{cases} \tag{19}$$

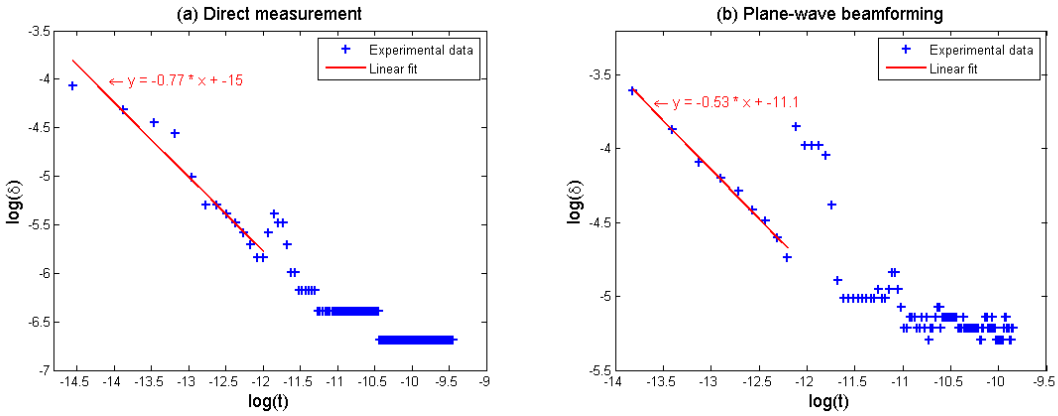

Figure 8. Verification of the diffusion approximation validity to determine the diffusion constant: (a) direct measurement; (b) plane-wave beamforming. The calculation of D is performed before the first back-surface echo. The two limitation phenomena occurring at long time are observed.

The same order of magnitude is obtained, which seems to show that the two methods are consistent. However, due to the higher signal-to-noise ratio and the better validation of the diffusion approximation condition, D_2 is probably more trustworthy. Yet we insist on the fact that these values are to be taken as orders of magnitude rather than precise measurements, given the limited range of time lags and the questionability of the diffusion approximation in that context. Other experimental techniques to characterise the diffusion constant exist. Particularly, a study of the time-of-flight function recorded in transmission is often used [4,12]. The comparison of our values with the results of these techniques in stainless steel samples could be interesting to do.

4. Conclusion

In this study, various post-processing techniques have been applied to the response matrix of a scattering medium, leading to the calculation of three parameters that are being used as entry parameters in an ultrasonic noise simulation method currently in progress at the CEA LIST. We showed that it is possible to obtain the elastic mean free path l_e, the correlation distance of the noise d_c, and the diffusion constant of the medium D by performing only one experimental measurement with a linear phased array. The main advantage of using the response matrix is that all information about the array and the inspected medium is contained in the impulse responses. It is then very easy to test other post-processing techniques without the need of carrying out other experiments. Another advantage is that fewer experiments are carried out and then more time can be devoted to post-processes. The main disadvantage, compared to measurements which are optimised for the calculation of a target parameter, is that going through the response matrix implies larger stored data and larger computation times.

The determination of all three parameters highlighted the difficulties dealing with the back-surface echoes. The presence of these echoes is needed to determine the elastic mean free path, but appears to be the main limitation when trying to calculate the correlation distance of the noise and the diffusion constant. Indeed, l_e characterise the coherent wave (i.e. the signal that resists to averaging processes), contrary to d_c and D that are related to the incoherent wave, and thus characterising the random noise that is classically eliminated by ensemble averaging.

Future work will study the link between dc and the microstucture, as well as refine the estimated values for D in similar samples. This will require either a new set of experiments with deeper samples, or, in order to study the short-time evolution of $\Delta\theta$, maybe develop a theoretical approach based on the radiative transfer equation, which is evidently much more complicate to handle than the simple diffusion approximation.

Finally, with the study of the coherent backscattering effect, we presented an alternative to the direct measurement of the backscattered ultrasonic intensity, by using plane-wave beamforming. Here again, the computation time is increased, but it comes with higher signal-to-noise ratio and greater angular resolution. Even if our arrays were not the best suited to emphasise this latter benefit due to the rapid saturation of the peak width, the use of larger ones can improve the quantitative determination of the diffusion constant and the study of the influence of back-surface echoes on the dynamic of the peak at longer times.

References

[1] Dorval V, Jenson F, Corneloup G and Moysan J 2010 *Review of Progress in QNDE* **29** 1309
[2] Feuilly N, Dupond O, Chassignole B et al., 2009 *Review of Progress in QNDE* **28** 1216
[3] Turner J A and Weaver R L 1994 *J. Acoust. Soc. Am.* **96** 3675
[4] Page J, Schriemer H P, Bailey A E and Weitz D A 1995 *Phys. Rev. E* **52** 3106
[5] Derode A and Fink M 1997 *J. Acoust. Soc. Am.* **101** 690
[6] Angelsen B 2000 *Ultrasound imaging: waves, signals and signals processing* (Trondheim: Emantec)
[7] Tourin A, Derode A, Peyre P and Fink M 2000 *J. Acoust. Soc. Am.* **108** 503
[8] Wu P and Stepinski 2000 *Ultrasonics* **38** 481
[9] Derode A, Tourin A and Fink M 2001 *Phys. Rev. E* **64** 036605
[10] Tourin A, Derode A, Roux P, van Tiggelen B A and Fink M 1997 *Phys. Rev. Lett.* **79** 3637
[11] Aubry A and Derode A 2007 *J. Acoust. Soc. Am.* **121** 70
[12] Anugonda P, Wiehn J S and Turner J A 2001 *Ultrasonics* **39** 429